Pt/CeO_2 with residual chloride as reusable soft Lewis acid catalysts: application to highly efficient isomerization of allylic esters

Qi-An Huang
Kyushu University
Asahi Haruta
Kyushu University
Yuhya Kumamoto
Kyushu University
Haruno Murayama (haruno9@chem.kyushu-univ.jp)
Kyushu University
Eiji Yamamoto
Kyushu University
Tetsuo Honma
Japan Synchrotron Radiation Research Institute (JASRI)/SPring-8
Mitsutaka Okumura
Osaka Univesity https://orcid.org/0000-0001-7403-1318
Hiroki Nobutou
Osaka University
Makoto Tokunaga
Kyushu University

Article

Keywords: Heterogeneous Acid and Base Catalysts, Highly Dispersed Supported Platinum Catalyst, Solvent-free Conditions, Pt-Cl bonds

Posted Date: January 19th, 2021

DOI: https://doi.org/10.21203/rs.3.rs-86545/v1

Abstract

Heterogeneous acid and base catalysts play a crucial role in many important chemical processes. Hard Lewis and Brønsted acid catalysts like silica-alumina and zeolites have been widely applied in numerous reactions; however, developing reusable and active soft Lewis acid catalysts remain a challenge. Herein, we demonstrate for the first time that a highly dispersed supported platinum catalyst can act as a heterogeneous soft Lewis acid. High turnover numbers and reusability were observed in the isomerization of allylic esters under solvent-free conditions. Moreover, the as-prepared catalysts are characterized by X-ray photoelectron spectroscopy (XPS) and X-ray absorption fine structure (XAFS) analyses, revealing that the highly dispersed Pt clusters with Pt–Cl bonds play a key role in the high activity. The residual chloride anion enhances the Lewis acidity of the Pt metal center and thus improves the catalytic activity. Simultaneously, the high catalytic activity of Pt/CeO_2 with residual chloride and the soft Lewis acid mechanism are also proved by density functional theory (DFT) calculations based on the model reaction.

Introduction

Supported platinum catalysts have been extensively researched and proven to play crucial roles in multiple applications, such as fuel cells[1,2], automotive three-way catalysts[3,4], catalytic redox reactions[5,6], and value-added fine chemical reactions[7,8]. Here, most applications of supported Pt catalysts are based on the redox function. In contrast, to the best of our knowledge, there are no reports on the supported Pt catalysts utilizing soft Lewis acidity, although homogenous Pt(II) complexes have been employed in the hydration of alkynes and nitriles[9–12], isomerization of allylbenzenes[13], cyclization of alkynes[14], etc. Thus, a heterogeneous supported platinum catalyst with soft Lewis acid function would be a promising practical catalyst.

According to Pearson's hard-soft acid-base (HSAB) principle, Lewis acids are classified into hard and soft acids which can activate corresponding hard or soft bases[15]. In many industrial reactions, zeolites, typical hard acids, have been widely used[16,17], including fluid catalytic cracking as commercial catalysts. On the other hand, most reactions based on soft Lewis acids have still been developed over homogeneous metal catalysts. The low-valent noble metals have soft characteristics and thus should function as a soft Lewis acid to activate soft bases, i.e., p electrons of C–C double and triple bonds, to undergo nucleophilic attack with various nucleophiles. Although these catalysts provide many useful synthetic applications, the poor reusability and small turnover numbers (TONs) hinder their practical utility; therefore, their applications remain limited.

Over the last decade, several catalytic reactions over recyclable supported Au nanoparticles as a soft Lewis acid were reported. Corma et al.[18,19], Parida et al.[20], and Zhao et al[21]. reported catalytic hydroamination with supported Au catalysts. Gryparis et al[22]. realized the cyclization of 1,6-enynes with TiO_2-supported Au nanoparticles. Toste and Somorjai et al[23]. also successfully used supported Au nanoparticles with N-heterocyclic carbene for lactonization. In Lewis acid-base catalysis, the

counteranion is important to expand the Lewis acid function. The stronger the conjugated acid of the counteranion is, the greater the Lewis acidity displayed by the central metal. Lewis acidity can also be enhanced when the cation is isolated, as in frustrated Lewis pairs[24]. However, soft cations such as Au(I) and Pd(II) are easily reduced to zero valences and easily aggregate, which makes it difficult to maintain activity when developing them as immobilized soft Lewis acids[25,26].

In recent years, considering the goal of atom efficiency and the scarcity of platinum resources, high-activity and low-cost platinum catalysts that contain highly dispersed Pt or even single-atom Pt catalysts have attracted widespread interest[27,28]. Moreover, a special strong metal-support interaction between Pt and CeO_2 was discovered and studied in-depth, revealing that the trapping of platinum on the CeO_2 surface can facilitate and sustain atomic dispersion[29–31]. Because of the particular properties of supported Pt in current applications, We infer that it is significant to performing research and development on supported Pt catalysts acting as soft Lewis acids.

Sustainable production of C4 chemicals is significant in industry[32]. During the series of catalytic reactions for C4 compounds, there are still several intermediate byproducts, such as but-3-ene-1,2-diyl diacetate (3,4-DABE) (Fig. 1a). 3,4-DABE is an isomer of but-2-ene-1,4-diyl diacetate (1,4-DABE), which is an important intermediate for the synthesis of tetrahydrofuran (THF). THF is produced million tons/year for polyesters and polyethers and several thousand tons/year of 3,4-DABE is wasted. The sustainable transformation of 3,4-DABE into 1,4-DABE will be valuable in industry and environmental protection and will be conducive to moving toward a low-carbon society.

In previous reports, several kinds of metal complex catalysts were developed for this reaction via the p-allyl intermediate[33,34] or soft Lewis acid mechanism[35,36] (Fig. 1b). Also, only low catalytic activity was obtained when testing hard Lewis acid catalysts like montmorillonite and ZSM-5, hence, we focus on developing efficient soft Lewis acid catalysts and thus choose the isomerization of 3,4-DABE as a model reaction.

In this research, for the first time, we report that Pt/CeO_2 with residual chloride can act as soft Lewis acids and can facilitate the efficient isomerization of allylic esters (Fig. 1c). Interestingly, the active species in this reaction are demonstrated as highly dispersed Pt clusters consisting of Pt–Cl and Pt–O bonds. Supported Pt catalysts with soft Lewis acid functionality were successfully developed, and the residual chloride anion enhanced the Lewis acidity of the Pt metal center. This should be the first example of the application of supported Pt soft Lewis acid catalysts. Also, this is the first use of supported noble catalysts in the isomerization of allylic esters. The active catalyst can be prepared via a simple impregnation method without complex fabrication steps. The reaction can be realized under solvent-free conditions, and the TON of the catalyst reaches 5400. The unique role of Pt–Cl bonds in the isomerization reaction was clearly explained by the results of the reaction and density functional theory (DFT) calculations. Furthermore, based on the success of this study, our findings introduce a new

approach for the valuable reaction of unsaturated compounds over high-performance supported Pt soft Lewis acid catalysts and provide a strategy to adjust the acidity of supported metal Lewis acid catalysts.

Results

Isomerization of 3,4-DABE. The direct transformation of 3,4-DABE to 1,4-DABE was investigated as a benchmark reaction for the isomerization of allylic esters using various heterogeneous catalysts. The equilibrium between 3,4-DABE and 1,4-DABE was determined to be 37/63[33], as shown in Fig. 2a. The distillation separation of 3,4- and 1,4-DABE is established in the industry. Catalyst screening was carried out with the metal oxide-supported Pd, Ir, Au, Pt catalysts, which may act as soft Lewis acids and facilitate the reaction based on the soft Lewis acid mechanism, according to the reported reaction with the Pd complex[36] and Au complex catalysts[35], where the highest TON is 33. To develop excellent active catalysts for the catalytic isomerization of allylic esters, we mainly chose ZrO_2 and CeO_2 as supports, which may promote the high dispersion of noble metal atoms on the surface, owing to the strong interaction[37,38]. Among the discussed supported noble metal catalysts, Au/ZrO_2 and Pt/CeO_2 afforded (2) in 11% and 52% yields, respectively (Supplementary Table 1). A high TON (5400) was also detected at the reaction scale of 10 mmol. With the optimized 1 wt% Pt/CeO_2, the isomerization reaction reached equilibrium after 30 min and obtained a turnover frequency (TOF) of 2120 h^{-1} with a catalyst amount of 0.05 mol% (Supplementary Figure 1). Pt/CeO_2 catalysts with Pt loadings less than 3 wt% showed high activity (Supplementary Table 2), which is probably related to the atomically dispersed Pt species that was only achieved with Pt loadings less than 3 wt%[39]. Pt/CeO_2 also exhibited better reusability than the other catalysts after reacting 3 times (Supplementary Figure 2). The optimized catalyst in this research is two orders of magnitude more active than previous catalysts (Fig. 2b).

The use of $H_2PtCl_6{\cdot}6H_2O$ as a precursor through the simple impregnation method could promote the creation of stable oxidized Pt species, such as PtO_xCl_y[40] and $Pt(OH)_xCl_y$[41]. Many reports on residual chloride in Pt catalysts revealed its poisoning effect on the catalytic activity[40,42]. Moreover, the promoting effect of the residual chloride was also investigated in a few cases[43]. To remove the influence of the residual chloride, we also examined Pt/CeO_2 prepared by Cl-free precursors, such as $Pt(acac)_2$ and $Pt(NH_3)_4(NO_3)_2$ (Table 1). The existence of chloride was confirmed by X-ray photoelectron spectroscopy (XPS) spectra (Fig. 3a). Cl-free Pt/CeO_2 showed no catalytic activities (Table 1, entries 2 and 3). In contrast, Pt/CeO_2 prepared from $H_2PtCl_6{\cdot}6H_2O$ and HCl-treated catalysts exhibited high catalytic activity, affording 1,4-DABE in approximately 60% yield (Table 1, entries 1, 4, and 5). The same effect was observed with the Pt/CeO_2-containing bromide anion. The reaction with CeO_2 treated by HCl was also investigated (Table 1, entry 6), and no yield for the target compounds was detected. Considering these results, the chloride anion enhanced the Lewis acidity of the Pt metal center, which is essential for the catalytic activity in this reaction.

Characterization of the Catalysts. High-angle annular dark-field scanning transmission electron microscopy (HAADF-STEM) coupled with energy-dispersive X-ray spectroscopy (EDS) mapping was used to determine the presence and size of Pt species on the prepared Pt/CeO_2 catalysts. The generation of Pt particles was not observed, which might be due to the high dispersion of Pt or the high atomic weight of Ce in the support.[37] Notably, the EDS mapping of Pt confirmed the high dispersity (Supplementary Figure 3). The existence and fine dispersion of chlorine atoms could also be detected from the EDS mapping of Cl.

To analyze the chemical state of the supported Pt species, the XPS spectra of the prepared catalysts were measured (Fig. 3). The quantification of the detected peaks and the spectra of Ce 3d regions are presented in the Supporting Information (Supplementary Table 4 and Figure 4). In the Cl 2p spectra shown in Fig. 3a, two peaks at 198.3 eV and 200 eV with a spin-orbit separation of 2 eV corresponding to $2p_{1/2}$ and $2p_{2/3}$ were observed for Pt/CeO_2_Cl, Pt/CeO_2_A_HCl, and Pt/CeO_2_N_HCl. The results reveal the existence of residual chloride ions in the catalysts prepared by $H_2PtCl_6 \cdot 6H_2O$ and Cl-free catalysts with HCl posttreatment. According to the reaction results, the crucial positive effect of chloride in Pt/CeO_2 catalysts was shown.

XPS spectra in the Pt 4f regions of Pt/CeO_2 prepared by various precursors and Cl-free catalysts with HCl posttreatment were collected and analyzed by peak deconvolution (Fig. 3b). From the spectra, Pt species on the surface of CeO_2 were primarily in the Pt^{2+} oxidation state (72.7 eV, Pt $4f_{7/2}$, $Pt(OH)_2$, yellow curves) with a component from Pt^{4+} (74.1 eV, Pt $4f_{7/2}$, PtO_2, blue curves) [44]. The invisible Pt nanoparticles in the HAADF-STEM image and the dominant Pt^{2+} oxidation state also support that most of the Pt atoms may be trapped and strongly bound on the CeO_2(111) facet by achieving 4-fold coordination[31,45]. For the catalysts containing chloride ions, the Pt^{4+}(Cl) component (74.8 eV, Pt $4f_{7/2}$, red curves) was noticed, considered as the Pt species with Pt–Cl bonds[40]. After HCl treatment, peaks attributed to Pt^{4+}(Cl) emerged. They appeared simultaneously with peaks for Cl 2p (198.3 eV, Cl $2p_{3/2}$). The ratio of Cl/Pt was roughly consistent with the ratio of Pt^{4+}(Cl)/Pt among the measured catalysts, supporting the assignment of the peak at 74.8 eV (Pt $4f_{7/2}$) as Pt^{4+}(Cl) (Table S2). Consequently, Pt/CeO_2 prepared from $H_2PtCl_6 \cdot 6H_2O$ and HCl-treated catalysts contains residual chloride ions, exhibiting high catalytic activity (Fig. 3c).

Pt L_{III}-edge X-ray absorption near edge structure (XANES) spectra of Pt foil and Pt/CeO_2 prepared by various precursors in an air atmosphere are shown in Fig. 4a. The characteristic peak, the white line, at 11568 eV was observed for the catalysts, which indicates that the Pt in the catalysts had high oxidation states[46]. The intensity of the white line for Pt/CeO_2_Cl was higher than those for Pt/CeO_2_A and

Pt/CeO_2_N. After HCl treatment, increased intensities of the white lines were observed in the spectra of Pt/CeO_2_A_HCl and Pt/CeO_2_A_HCl, revealing the increased oxidation state related to the generation of chloride (Fig. 4c).

In phase-uncorrected radial structure functions (RSFs) for Pt/CeO_2 prepared by various precursors (Fig. 4b), two peaks were mainly observed at approximately 1.65 Å and 1.95 Å in Pt/CeO_2_Cl. Compared with the peaks of the reference sample of Pt foil, PtO_2, and K_2PtCl_6, the peak at approximately 1.65 Å were attributed to Pt–O coordination, and the peak at approximately 1.95 Å was attributed to Pt–Cl coordination. The weak peak intensities at 2.60 Å and 2.85 Å, corresponding to the Pt–Pt coordination distance in Pt foil and the Pt–O–Pt coordination distance in PtO_2, respectively, were much smaller than those of the reference compounds, supporting the high dispersion of Pt species and the formation of Pt nanoclusters or even atomic Pt species. This finding was also consistent with the results of HAADF-TEM. In the spectra of Pt/CeO_2_A and Pt/CeO_2_N, peaks at approximately 1.65 Å and 2.85 Å were observed, and almost no peaks at approximately 1.95 Å were found, revealing the generation of PtO_x species. After HCl treatment, in the spectra of Pt/CeO_2_A_HCl and Pt/CeO_2_N_HCl, peaks at approximately 1.65 Å and 1.95 Å were observed (Fig. 4d). No obvious peaks were found around the distances of other bonds. Considering the reaction results and the XPS spectra, the active species were proven to contain both Pt–O and Pt–Cl that were highly dispersed. Additionally, the k^3-weighted Pt L_{III}-edge extended X-ray absorption fine structure (EXAFS) oscillation patterns of Pt/CeO_2_Cl, Pt/CeO_2_A_HCl, and Pt/CeO_2_N_HCl were compared with those of PtO_2, $Na_2Pt(OH)_6$ and K_2PtCl_6 (Supplementary Figure 5). The oscillation patterns of Pt/CeO_2_Cl, Pt/CeO_2_A_HCl, and Pt/CeO_2_N_HCl were between those of K_2PtCl_6 and PtO_2, supporting the existence of Pt–O coordination and Pt–Cl coordination in the active catalysts.

Furthermore, the structural parameters of the Pt/CeO_2 catalysts discussed above were obtained by EXAFS curve-fitting analysis (Supplementary Table 5). The coordination numbers (CNs) of Pt–O for the first shell of the Pt/CeO_2 catalyst prepared from three kinds of precursors were approximately between 3 and 4. For Pt/CeO_2_Cl, the CN value of Pt–Cl was 1.49 ± 0.78. After HCl treatment, the CN values of Pt–Cl were approximately 1.76 ± 1.03 (Pt/CeO_2_A_HCl) and 1.79 ± 0.27 (Pt/CeO_2_N_HCl). A similar CN ratio (x/y, PtO_xCl_y) between Pt–O and Pt–Cl of approximately 2.4 was found for Pt/CeO_2_Cl and Pt/CeO_2_A_HCl. For Pt/CeO_2_N_HCl, the ratio was approximately 1.2. This result also correlated with the observation of $Pt(OH)_xCl_y$ and PtO_xCl_y.

For further investigation, Pt L_{III}-edge XANES spectra of Pt catalysts supported by various metal oxides were measured in an air atmosphere. Estimating the intensities of the white lines, the oxidation states of Pt species supported on other metal oxides were lower than those on CeO_2 (Supplementary Figure 6). Pt–O and Pt–Cl bonds were also detected in the phase-uncorrected RSFs of these catalysts, and a relatively low intensity was observed for the catalysts with low catalytic activity. The oxidation state of Pt species in the catalysts was analyzed by the edge energy of Pt L_I-edge XANES spectra (Supplementary Figure 7).

The oxidation states of Pt in Pt/CeO_2_Cl were nearly 4+ and higher compared with those of Pt/Al_2O_3_Cl. These results suggest that a higher oxidation state of Pt shows higher catalytic activity.

Moreover, the structural parameters of Cl-containing Pt catalysts supported by other metal oxides were also estimated by curve-fitting analysis (Supplementary Table 5). Although the CN value of Pt–Cl in Pt/ZrO_2_Cl was similar to that of Pt/CeO_2_Cl, the CN value of Pt–O was much lower than that of Pt/CeO_2_Cl. Summarizing the above results, the high oxidation state, CN value of Pt–Cl and dispersity were core factors affecting the catalytic activity, and CeO_2 could help the Pt species on its surface maintain a high oxidation state and dispersity[45,47].

Hydrogen temperature-programmed reduction (H_2-TPR) was performed to investigate the active Pt species (Supplementary Figure 8&9). Active Pt species were mainly considered $Pt(OH)_xCl_y$ and PtO_xCl_y with the reference peaks obtained[48–50]. This result was consistent with the result of the EXAFS spectra. The shift in the temperature may be related to the difference in the ratio of x/y of the species. Based on the above experimental results, the formed Pt–Cl bonds in Pt/CeO_2 catalysts play an essential role in the high catalytic activity, which should be due to the stably enhanced acidity of Pt in the presence of chloride anions. The active species on CeO_2 are considered $Pt(OH)_xCl_y$ and PtO_xCl_y, which can be obtained from a simple impregnation method or HCl posttreatment. Also, because of the strong interaction between Pt and CeO_2, Pt-Cl clusters can easily be highly dispersed and help Pt maintain a high oxidation state.

Catalytic Isomerization of Allylic Esters. The reaction mechanism of the catalytic isomerization of allylic esters could be primarily classified into the p-allyl intermediate mechanism and the soft Lewis acid mechanism. Pentanoic acid was added to the reaction system to confirm the actual mechanism of the reaction using Pt/CeO_2 catalysts. Only the products of (*E*)-**2a** and (*Z*)-**2a** were detected after the reaction, no exchange between externally added pentanoic acid, demonstrating that the mechanism for the isomerization of allylic esters over Pt/CeO_2 should be a soft Lewis acid mechanism (Fig. 5).

A substrate scope investigation was carried out under the optimized reaction conditions. The prepared active Pt/CeO_2 catalysts also provided excellent reaction activity for the catalytic isomerization of other allylic acetates (Supplementary Figure 10) and allylic benzoates (Supplementary Figure 11). Homogeneous Pt and Pd catalysts were also examined for allylic benzoate (results listed in Supplementary Table 6). The soft Lewis acid complexes including $PdCl_2(MeCN)_2$ afforded the product for allylic benzoate as well as Pt/CeO_2 although TON was low (5000 for Pt/CeO_2 cf. 6 for $PdCl_2(MeCN)_2$). It is noteworthy that Pd(0) and Pt(0) complexes, that can catalyze the reaction through a p-allyl intermediate, only gave eliminated diene due to the low nucleophilicity of benzoate. These results also supported the soft Lewis acid mechanism for Pt/CeO_2 catalysts.

The proposed catalytic cycle for the isomerization of allylic esters was presented, and the hexatomic ring state on the Pt catalysts was considered to be a transition state (Supplementary Figure 12).

Result of Calculations. Since the Pt-Cl clusters supported by metal oxides were confirmed as the active species for the catalytic isomerization of allylic esters, the quantum chemical calculation was utilized to investigate the role of the charge on Pt clusters. Fig. 6 illustrates the typical reaction profile for the catalytic isomerization of allylic esters based on cationic Pt cluster model systems.

Primarily, DFT calculations on the isolated cluster model were performed with Gaussian09 to discuss the relationship between the activation energies and the charge of the Pt cluster. The calculation results of the reaction process based on the cluster model agreed with the proposed Lewis acid mechanism, and INI-TS1 was considered the activation energy barrier because of the major energy gap between TS1 and INI (Fig. 6a). In other words, the catalytic activities of cationic clusters are much better than those of neutral clusters. The detailed results are not shown here. The change in energy of the transition state corresponds to a reversible reaction.

Afterward, a slab model was built with single-atom tetravalent Pt species containing Pt–Cl bonds and Pt–O bonds on CeO_2(111) surfaces to further simulate the actual reaction path (Fig. 6b), such as $PtOCl_2/CeO_2$, $PtCl_4/CeO_2$, and PtO_2/CeO_2 with VASP code. Cl–Ce bonding was observed in the optimized model of $PtCl_4/CeO_2$, where the Cl–Ce group can act as a Lewis acid and thus likely enhance the acidity of the Pt metal center in the Lewis acid-assisted approach[51,52]. The energy of each state for the whole process was optimized, and the diagram of the results shows that the activation energy barrier and adsorption-desorption energy were small enough to facilitate this reaction when using Pt/CeO_2 catalysts containing Pt–Cl bonds (Fig. 6c). Additionally, the calculation of the reaction over PtO_2/CeO_2 was performed, and the result reveals that the adsorption of 3,4-DABE should occur via di–σ (Pt-O) bonding between the C=C and Pt–O instead of the p-bond (Fig. 6d). Because of the large activation energy barrier (1.40 eV) and high desorption energy (2.14 eV), PtO_2/CeO_2 was proven to show low activity for this kind of reaction (see the Supporting Information for computational details). The results of DFT calculations are basically consistent with the results of the reaction and characterization experiments. This finding should promote the understanding of the effects of the fine structure or composition of supported platinum catalysts on catalytic organic reactions based on olefin compounds.

Conclusion

In conclusion, the effective isomerization of allylic esters was realized under solvent-free conditions over metal oxide-supported Pt catalysts, which can act as soft Lewis acids. Stable reusability, a high TON (up to 5400), and a wide substrate scope are confirmed with optimized Pt catalysts. With the aid of structural characterizations, the active species on CeO_2 were detected as Pt oxide clusters containing Pt–Cl bonds, such as PtO_xCl_y. The reaction process with the prepared Pt catalysts was proven to be based on the soft Lewis acid mechanism, as revealed by experiments and DFT calculations. The analysis results show that Pt–Cl bonds, the high oxidation state of Pt, and the strong interaction between the support and Pt play crucial roles in the high activity of supported Pt catalysts in this reaction. This research provides valuable examples of supported Pt soft Lewis acids that can directly catalyze the isomerization of allylic esters

under simple conditions. Moreover, the essential role of the residual chloride anion and its enhancement effect on the Lewis acidity of the Pt metal center and thus the high catalytic activity should also be significant for heterogeneous catalyst design in the future.

Method

Materials. Chloroplatinic acid hexahydrate ($H_2PtCl_6·6H_2O$) was purchased from Furuya Metal Co., Ltd. Palladium nitrate ($Pd(NO_3)_2$) and hydrogen tetrachloroaurate tetrahydrate ($HAuCl_4•4H_2O$) were purchased from Tanaka Precious Metal Co., Ltd. Platinum acetylacetonate ($Pt(acac)_2$), tetraammineplatinum(II) nitrate ($Pt(NH_3)_4(NO_3)_2$), and hydrogen hexachloroiridate(IV) n-hydrate ($H_2IrCl_6·nH_2O$) were purchased from Wako Pure Chemical Industries. CeO_2 (JRC-CEO-3, 81 m^2/g) and ZrO_2 (JRC-ZRO-4, 30 m^2/g) were Japan reference catalysts supplied by the Catalysts Society of Japan. Al_2O_3 with a specific surface area of 179 m^2/g was purchased from Mizusawa Industrial Chemicals, Ltd. MgO with a specific surface area of 8 m^2/g was purchased from Ube Industries, Ltd. TiO_2 (PC-101) was purchased from Titan Kogyo, Ltd. 3,4-DABE was purchased from Wako Pure Chemical Industries and used as received. All chemicals were used without further purification.

Catalyst Preparation. Pt/CeO_2, Pt/ZrO_2, Pt/Al_2O_3, Pt/TiO_2, and Pt/MgO catalysts with a Pt loading of 1 wt% were prepared by the impregnation method. H_2PtCl_6 aqueous solution (Pt: 19.75 g/L; 511 μL) was diluted in 1.5 mL distilled water. A metal oxide support (1.0 g) was added to the aqueous solution and stirred at room temperature for 30 min. After the impregnation process was complete, the catalysts were dried via a vacuum freeze method overnight. Then, the catalysts were calcined in a furnace at 300 ℃ for 4 h. Pt/CeO_2 Cl-free catalysts were also prepared by the impregnation method from $Pt(acac)_2$ and $Pt(NH_3)_4(NO_3)_2$ and were named Pt/CeO_2_A and Pt/CeO_2_N, respectively. $Pt(acac)_2$ (20.4 mg) was dissolved in 2 mL dehydrated toluene, and the following procedures were as described above. $Pt(NH_3)_4(NO_3)_2$ (20.1 mg) was dissolved in 2 mL 0.5 M HNO_3. The following procedures were the same as described above.

Ir/CeO_2 catalysts were prepared by the impregnation method. $H_2IrCl_6·nH_2O$ (Ir: 36.5 wt%; 27.7 mg) was diluted in 1.5 mL distilled water. The following procedures were the same as described above.

Pd/CeO_2 and Pd/ZrO_2 catalysts were prepared by the impregnation method. $Pd(NO_3)_2$ aqueous solution (Pd: 200 g/L) was diluted in a small amount of water. ZrO_2 or CeO_2 (1.0 g) was added to the aqueous solution and stirred at RT for 30 min. After the impregnation process was complete, H_2O was removed by freeze-drying. The obtained catalysts were calcined at 550 °C for 4 h and then reduced in a flow of pure H_2 (20 mL/min) at 200 °C for 2 h to obtain Pd/CeO_2 or Pd/ZrO_2.

Au/ZrO_2 was prepared by homogeneous deposition–precipitation (HDP). ZrO_2 (1.0 g) was added to an aqueous solution (100 mL) of $HAuCl_4•4H_2O$ (21.1 mg) and urea (7.6 g). The mixture was stirred at 90 °C

for 10 h. The solid was collected by filtration, washed with water, and dried in air at 70 °C overnight. The solid was calcined in air at 300 °C for 4 h and used for catalytic reactions without further treatment.

HCl treatment was performed with Pt/CeO_2 catalysts prepared by Cl-free precursors. Treated catalysts were named Pt/CeO_2_A_HCl and Pt/CeO_2_N_HCl. The prepared catalysts (100 mg) were added into a 0.1 M HCl solution (1.5 mL) and stirred at 90 ℃ for 6 h. The solid was filtered and vacuum freeze-dried for 4 h. The obtained catalysts were calcined again at 300 ℃ for 1 h.

Characterization. HAADF-STEM images were acquired with a JEOL JEM-ARM200F operated at 200 kV. The loading amount of Pt in the prepared catalysts was determined by microwave plasma-atomic emission spectrometry (MP-AES) via an Agilent 4100 MP-AES instrument. Powder X-ray diffraction (XRD) was performed using a Rigaku MiniFlex600 instrument equipped with a Cu K_α radiation source. The nature of the surface species was analyzed by XPS using a Shimadzu AXIS-165 spectrometer equipped with Al K_α radiation at a pressure lower than 10^{-6} Pa. The obtained binding energies were calibrated to the C1s peak at 284.8 eV. XPS spectra were further analyzed using XPS PEAK41 software. The local structures of Pt species were analyzed by Pt L_{III}-edge XAFS spectra collected at the BL14B2 beamline of Spring-8 (Hyogo, Japan) [53,54]. XAFS measurement experiments were conducted in fluorescence mode. The specific spectral analysis was performed using the XAFS analysis software Athena and REX2000. Temperature-programmed reduction of H_2 (H_2-TPR) was analyzed using a BELCAT instrument equipped with a thermal conductivity detector (TCD).

Conversions and yields of the compounds discussed were analyzed by gas chromatography (GC) using an Agilent GC 6850 Series II instrument equipped with a flame ionization detector (FID) and a J&W HP-1 column using tridecane as an internal standard. ^1H and ^{13}C NMR spectra were analyzed on a JEOL JNM-ECS400 or JEOL JNM-ECA600 spectrometer.

General Procedure for the Catalytic Reactions. A glass tube was charged with 1 wt% supported Pt catalysts (Pt 0.01 mol%, 2.0 mg; Pt 0.05 mol%, 9.8 mg; Pt 0.15 mol%, 29.3 mg), but-3-ene-1,2-diyl diacetate (1 mmol) and a magnetic stirring bar. The reaction mixture was stirred at 150 ℃ under an N_2 or air atmosphere (1 atm). After the reaction, the mixture was filtered, and the filtrate was analyzed by GC using tridecane as an internal standard. In the large-scale reaction of 10 mmol, 19.5 mg (Pt 0.01 mol%) Pt/CeO_2, but-3-ene-1,2-diyl diacetate (10 mmol), and a magnetic stirring bar were added to the glass tube, and the catalytic activity was tested through the same method mentioned above. In a recycling experiment, a glass tube was charged with 1 wt% Pt/CeO_2 catalysts (0.15 mol%, 29.3 mg), but-3-ene-1,2-diyl diacetate (1 mmol) and a magnetic stirring bar. The catalytic activity was tested through the same method mentioned above. The glass tube was cooled in an ice bath for approximately 20 min after reacting for 2 h. The Pt catalysts were washed with Et_2O, collected by centrifugation, and dried under vacuum conditions. Then, the obtained Pt catalysts were used for the next reaction.

Computational Methods. DFT calculations for the model cluster systems were carried out using Gaussian 09[55]. For the model clusters, a 6-31+G(d) basis set for C, O, and H atoms and LANL2DZ for Pt atoms were used, and hybrid DFT (PBE0 functional) was applied. First-principles calculations using DFT for the structures and electronic states of the slab models were carried out with the Vienna Ab initio Simulation Package (VASP) [56,57]. The projector-augmented-wave (PAW)[58] method was utilized for the calculation of the ionic core electrons. The Perdew-Burke-Ernzerhof (PBE)[59] functional with a cutoff energy of 400 eV was set for the determination of the exchange-correlation term. To confirm the possible behavior of electrons in the supported Pt catalysts, the DFT + U method (U (Ce, 4f)=5.0 eV) was used[60].

Data availability

The data that support the findings of this study are available from the corresponding authors on reasonable request.

References

(1) Bing, Y.; Liu, H.; Zhang, L.; Ghosh, D.; Zhang, J. Nanostructured Pt-Alloy Electrocatalysts for PEM Fuel Cell Oxygen Reduction Reaction. *Chem. Soc. Rev.* **39**, 2184–2202 (2010).

(2) Debe, M. K. Electrocatalyst Approaches and Challenges for Automotive Fuel Cells. *Nature* **486**, 43–51 (2012).

(3) Nibbelke, R. H.; Nievergeld, A. J. L.; Hoebink, J. H. B. J.; Marin, G. B. Development of a Transient Kinetic Model for the CO Oxidation by O_2 over a Pt/Rh/CeO2/γ-Al_2O_3 Three-Way Catalyst. *Appl. Catal. B Environ.* **19**, 245–259 (1998).

(4) Tanaka, H.; Taniguchi, M.; Uenishi, M.; Kajita, N.; Tan, I.; Nishihata, Y.; Mizuki, J.; Narita, K.; Kimura, M.; Kaneko, K. Self-Regenerating Rh- and Pt-Based Perovskite Catalysts for Automotive-Emissions Control. *Angew. Chem. Int. Ed.* **45,** 5998–6002 (2006).

(5) Ding, K.; Gulec, A.; Johnson, A. M.; Schweitzer, N. M.; Stucky, G. D.; Marks, L. D.; Stair, P. C. Identification of Active Sites in CO Oxidation and Water-Gas Shift over Supported Pt Catalysts. *Science* **350**, 189–192 (2015).

(6) Kuwahara, Y.; Yoshimura, Y.; Haematsu, K.; Yamashita, H. Mild Deoxygenation of Sulfoxides over Plasmonic Molybdenum Oxide Hybrid with Dramatic Activity Enhancement under Visible Light. *J. Am. Chem. Soc.* **140**, 9203–9210 (2018).

(7) Chen, C. B.; Chen, M. Y.; Zada, B.; Ma, Y. J.; Yan, L.; Xu, Q.; Li, W. zhi; Guo, Q. X.; Fu, Y. Effective Conversion of Biomass-Derived Ethyl Levulinate into γ-Valerolactone over Commercial Zeolite Supported Pt Catalysts. *RSC Adv.* **6**, 112477–112485 (2016).

(8) Siddiki, S. M. A. H.; Touchy, A. S.; Jamil, M. A. R.; Toyao, T.; Shimizu, K. I. C -Methylation of Alcohols, Ketones, and Indoles with Methanol Using Heterogeneous Platinum Catalysts. *ACS Catal.* **8**, 3091–3103 (2018).

(9) Hartman, J. W., Hiscox, W. C. & Jennings, P. W. Catalytic Hydration of Alkynes with Platinum(II) Complexes. *J. Org. Chem.* **58**, 7613–7614 (1993).

(10) Jiang, X. Bin, Minnaard, A. J., Feringa, B. L. & De Vries, J. G. Platinum-Catalyzed Selective Hydration of Hindered Nitriles and Nitriles with Acid- or Base-Sensitive Groups. *J. Org. Chem.* **69**, 2327–2331 (2004).

(11) Lucey, D. W. & Atwood, J. D. Insight into the selective room-temperature platinum(II) catalytic hydration of alkynes in water. *Organometallics* **21**, 2481–2490 (2002).

(12) Xing, X. et al. Highly Active Platinum Catalysts for Nitrile and Cyanohydrin Hydration: Catalyst Design and Ligand Screening via High-Throughput Techniques. *J. Am. Chem. Soc.* **140**, 17782–17789 (2018).

(13) Scarso, A.; Colladon, M.; Sgarbossa, P.; Santo, C.; Michelin, R. A.; Strukul, G. Highly Active and Selective Platinum(II)-Catalyzed Isomerization of Allylbenzenes: Efficient Access to (E)-Anethole and Other Fragrances via Unusual Agostic Intermediates. *Organometallics* **29**, 1487–1497 (2010).

(14) Bhanu Prasad, B. A., Yoshimoto, F. K. & Sarpong, R. Pt-catalyzed pentannulations from in situ generated metallo-carbenoids utilizing propargylic esters. *J. Am. Chem. Soc.* **127**, 12468–12469 (2005).

(15) Pearson, R. G. Absolute Electronegativity and Absolute Hardness of Lewis Acids and Bases. *J. Am. Chem. Soc*. **107**, 6801–6806 (1985).

(16) Dapsens, P. Y., Mondelli, C. & Pérez-Ramírez, J. Design of Lewis-acid centres in zeolitic matrices for the conversion of renewables. *Chem. Soc. Rev*. **44**, 7025–7043 (2015).

(17) Li, Y., Li, L. & Yu, J. Applications of Zeolites in Sustainable Chemistry. *Chem* **3**, 928–949 (2017).

(18) Corma, A.; González-Arellano, C.; Iglesias, M.; Navarro, M. T.; Sánchez, F. Synthesis of Bifunctional Au-Sn Organic-Inorganic Catalysts for Acid-Free Hydroamination Reactions. *Chem. Commun*. **46**, 6218–6220 (2008).

(19) Corma, A.; Concepción, P.; Domínguez, I.; Forné, V.; Sabater, M. J. Gold Supported on a Biopolymer (Chitosan) Catalyzes the Regioselective Hydroamination of Alkynes. *J. Catal*. **251**, 39–47 (2007).

(20) Sahoo, M.; Parida, K. Facile Fabrication of Organic-Inorganic Hybrid Material Based on Well-Dispersed AuNPs on Organo-Functionalised Zn-Al-Layered Double Hydroxides for Hydroamination of 1-Hexene. *ChemistrySelect* **3**, 3092–3100 (2018).

(21) Lee, L. C.; Zhao, Y. Room Temperature Hydroamination of Alkynes Catalyzed by Gold Clusters in Interfacially Cross-Linked Reverse Micelles. *ACS Catal.* **4**, 688–691 (2014).

(22) Gryparis, C.; Efe, C.; Raptis, C.; Lykakis, I. N.; Stratakis, M. Cyclization of 1,6-Enynes Catalyzed by Gold Nanoparticles Supported on TiO_2: Significant Changes in Selectivity and Mechanism, as Compared to Homogeneous Au-Catalysis. *Org. Lett.* **14**, 2956–2959 (2012).

(23) Ye, R.; Zhukhovitskiy, A. V.; Kazantsev, R. V.; Fakra, S. C.; Wickemeyer, B. B.; Toste, F. D.; Somorjai, G. A. Supported Au Nanoparticles with N-Heterocyclic Carbene Ligands as Active and Stable Heterogeneous Catalysts for Lactonization. *J. Am. Chem. Soc.* **140**, 4144–4149 (2018).

(24) Stephan, D. W. Frustrated Lewis Pairs. *J. Am. Chem. Soc.* **137**, 10018–10032 (2015).

(25) Cai, R.; Ye, X.; Sun, Q.; He, Q.; He, Y.; Ma, S.; Shi, X. Anchoring Triazole-Gold(I) Complex into Porous Organic Polymer to Boost the Stability and Reactivity of Gold(I) Catalyst. *ACS Catal.* **7**, 1087–1092 (2017).

(26) Otake, K. I.; Ye, J.; Mandal, M.; Islamoglu, T.; Buru, C. T.; Hupp, J. T.; Delferro, M.; Truhlar, D. G.; Cramer, C. J.; Farha, O. K. Enhanced Activity of Heterogeneous Pd(II) Catalysts on Acid-Functionalized Metal-Organic Frameworks. *ACS Catal.* **9**, 5383–5390 (2019).

(27) Tang, Z.; Liu, P.; Cao, H.; Bals, S.; Heeres, H. J.; Pescarmona, P. P. Pt/ZrO_2 Prepared by Atomic Trapping: An Efficient Catalyst for the Conversion of Glycerol to Lactic Acid with Concomitant Transfer Hydrogenation of Cyclohexene. *ACS Catal.* **9**, 9953–9963 (2019).

(28) Nie, L.; Mei, D.; Xiong, H.; Peng, B.; Ren, Z.; Hernandez, X. I. P.; DeLaRiva, A.; Wang, M.; Engelhard, M. H.; Kovarik, L.; et al. Activation of Surface Lattice Oxygen in Single-Atom Pt/CeO_2 for Low-Temperature CO Oxidation. *Science* **358**, 1419–1423 (2017).

(29) Daelman, N.; Capdevila-Cortada, M.; López, N. Dynamic Charge and Oxidation State of Pt/CeO_2 Single-Atom Catalysts. *Nat. Mater.* **18**, 1215–1221 (2019).

(30) Pereira-Hernández, X. I.; DeLaRiva, A.; Muravev, V.; Kunwar, D.; Xiong, H.; Sudduth, B.; Engelhard, M.; Kovarik, L.; Hensen, E. J. M.; Wang, Y.; et al. Tuning $Pt\text{-}CeO_2$ Interactions by High-Temperature Vapor-Phase Synthesis for Improved Reducibility of Lattice Oxygen. *Nat. Commun.* **10**, 1358 (2019).

(31) Dvořák, F.; Camellone, M. F.; Tovt, A.; Tran, N. D.; Negreiros, F. R.; Vorokhta, M.; Skála, T.; Matolínová, I.; Mysliveček, J.; Matolín, V.; et al. Creating Single-Atom Pt-Ceria Catalysts by Surface Step Decoration. *Nat. Commun.* 2016, 7. 10801.

(32) Li, X.; Jia, P.; Wang, T. Furfural: A Promising Platform Compound for Sustainable Production of C4 and C5 Chemicals. *ACS Catal.* **6**, 7621–7640 (2016).

(33) Bouquillon, S.; Muzart, J. Palladium(0)-Catalyzed Isomerization of (Z)-1,4-Diacetoxy-2-Butene - Dependence of η1- or η3-Allylpalladium as a Key Intermediate on the Solvent Polarity. *Eur. J. Org. Chem.* **17**, 3301–3305 (2001).

(34) Mukhopadhyay, M.; Reddy, M. M.; Maikap, G. C.; Iqbal, J. Cobalt(II)-Catalyzed Conversion of Allylic Alcohols/Acetates to Allylic Amides in the Presence of Nitriles. *J. Org. Chem.* **60**, 2670–2676 (1995).

(35) Marion, N.; Gealageas, R.; Nolan, S. P. [(NHC)Au1]-Catalyzed Rearrangement of Allylic Acetates. *Org. Lett.* **9**, 2653–2656 (2007).

(36) Zawisza, A. M.; Bouquillon, S.; Muzart, J. Palladium(II)-Catalyzed Isomerization of (Z)-1,4-Diacetoxy-2-Butene: Solvent Effects. *Eur. J. Org. Chem.* **2**, 3901–3904 (2007).

(37) Ishida, T.; Honma, T.; Nakada, K.; Murayama, H.; Mamba, T.; Kume, K.; Izawa, Y.; Utsunomiya, M.; Tokunaga, M. Pd-Catalyzed Decarbonylation of Furfural: Elucidation of Support Effect on Pd Size and Catalytic Activity Using in-Situ XAFS. *J. Catal.* **374**, 320–327 (2019).

(38) Datye, A. K.; Jones, J.; Pereira Hernandez, X. I.; Challa, S. R.; Pham, H.; Oh, S.; Qi, G.; Wiebenga, M. H.; Xiong, H.; DeLaRiva, A. T.; et al. Thermally Stable Single-Atom Platinum-on-Ceria Catalysts via Atom Trapping. *Science* **353**, 150–154 (2016).

(39) Kunwar, D.; Zhou, S.; Delariva, A.; Peterson, E. J.; Xiong, H.; Pereira-Hernández, X. I.; Purdy, S. C.; Ter Veen, R.; Brongersma, H. H.; Miller, J. T.; et al. Stabilizing High Metal Loadings of Thermally Stable Platinum Single Atoms on an Industrial Catalyst Support. *ACS Catal.* **9**, 3978–3990 (2019).

(40) Gracia, F. J.; Miller, J. T.; Kropf, A. J.; Wolf, E. E. Kinetics, FTIR, and Controlled Atmosphere EXAFS Study of the Effect of Chloride on Pt-Supported Catalysts during Oxidation Reactions. *J. Catal.* **209**, 341–354 (2002).

(41) Ismagilov, Z. R.; Yashnik, S. A.; Startsev, A. N.; Boronin, A. I.; Stadnichenko, A. I.; Kriventsov, V. V.; Kasztelan, S.; Guillaume, D.; Makkee, M.; Moulijn, J. A. Deep Desulphurization of Diesel Fuels on Bifunctional Monolithic Nanostructured Pt-Zeolite Catalysts. *Catal. Today* **144**, 235–250 (2009).

(42) Zhu, X.; Cheng, B.; Yu, J.; Ho, W. Halogen Poisoning Effect of Pt-TiO_2 for Formaldehyde Catalytic Oxidation Performance at Room Temperature. *Appl. Surf. Sci.* **364**, 808–814 (2016).

(43) Shi, H.; Gutiérrez, O. Y.; Yang, H.; Browning, N. D.; Haller, G. L.; Lercher, J. A. Catalytic Consequences of Particle Size and Chloride Promotion in the Ring-Opening of Cyclopentane on Pt/Al_2O_3. *ACS Catal.* **3**, 328–338 (2013).

(44) Lee, J.; Ryou, Y.; Chan, X.; Kim, T. J.; Kim, D. H. How Pt Interacts with CeO_2 under the Reducing and Oxidizing Environments at Elevated Temperature: The Origin of Improved Thermal Stability of Pt/CeO_2 Compared to CeO_2. *J. Phys. Chem. C* **120**, 25870–25879 (2016).

(45) Bruix, A.; Rodriguez, J. A.; Ramírez, P. J.; Senanayake, S. D.; Evans, J.; Park, J. B.; Stacchiola, D.; Liu, P.; Hrbek, J.; Illas, F. A New Type of Strong Metal-Support Interaction and the Production of H_2 through the Transformation of Water on $Pt/CeO_2(111)$ and $Pt/CeO_x/TiO_2(110)$ Catalysts. *J. Am. Chem. Soc.* **134**, 8968–8974 (2012).

(46) Brown, M.; Peierls, R. E.; Stern, E. A. White Lines in X-ray Absorption. *Phys. Rev. B* **15**, 738–744 (1977).

(47) Bruix, A.; Lykhach, Y.; Matolínová, I.; Neitzel, A.; Skála, T.; Tsud, N.; Vorokhta, M.; Stetsovych, V.; Ševčíková, K.; Mysliveček, J.; et al. Maximum Noble-Metal Efficiency in Catalytic Materials: Atomically Dispersed Surface Platinum. *Angew. Chem. Int. Ed.* **53**, 10525–10530 (2014).

(48) Lieske, H.; Lietz, G.; Spindler, H.; Völter, J. Reactions of Platinum in Oxygen- and Hydrogen-Treated Pt γ-Al_2O_3 catalysts. I. Temperature-Programmed Reduction, Adsorption, and Redispersion of Platinum. *J. Catal.* **81**, 8–16 (1983).

(49) Gao, Y.; Wang, W.; Chang, S.; Huang, W. Morphology Effect of CeO_2 Support in the Preparation, Metal-Support Interaction, and Catalytic Performance of Pt/CeO_2 Catalysts. *ChemCatChem* **5**, 3610–3620 (2013).

(50) Acerbi, N.; Tsang, S. C. E.; Jones, G.; Golunski, S.; Collier, P. Rationalization of Interactions in Precious Metal/Ceria Catalysts Using the d-Band Center Model. *Angew. Chem. Int. Ed.* **52**, 7737–7741 (2013).

(51) Hu, Z.; Metiu, H. Halogen Adsorption on CeO_2: The Role of Lewis Acid-Base Pairing. *J. Phys. Chem. C* **116**, 6664–6671 (2012).

(52) Futatsugi, K.; Yamamoto, H. Oxazaborolidine-Derived Lewis Acid Assisted Lewis Acid as a Moisture-Tolerant Catalyst for Enantioselective Diels-Alder Reactions. *Angew. Chem. Int. Ed.* **44**, 1484–1487 (2005).

(53) Honma, T.; Oji, H.; Hirayama, S.; Taniguchi, Y.; Ofuchi, H.; Takagaki, M. Full-Automatic XAFS Measurement System of the Engineering Science Research II Beamline BL14B2 at SPring-8. *AIP Conf. Proc.* **1234**, 13–16 (2010).

(54) Oji, H.; Taniguchi, Y.; Hirayama, S.; Ofuchi, H.; Takagaki, M.; Honma, T. Automatic XAFS Measurement System Developed at BL14B2 in SPring-8. J. *Synchrotron Radiat.* **19**, 54–59 (2012).

(55) Gaussian 09, Revision A.02, M. J. Frisch, G. W. Trucks, H. B. Schlegel, G. E. Scuseria, M. A. Robb, J. R. Cheeseman, G. Scalmani, V. Barone, G. A. Petersson, H. Nakatsuji, X. Li, M. Caricato, A. Marenich, J. Bloino, B. G. Janesko, R. Gomperts, B. Mennucci, H. P. Hratchian, J. V. Ortiz, A. F. Izmaylov, J. L. Sonnenberg, D. Williams-Young, F. Ding, F. Lipparini, F. Egidi, J. Goings, B. Peng, A. Petrone, T. Henderson, D. Ranasinghe, V. G. Zakrzewski, J. Gao, N. Rega, G. Zheng, W. Liang, M. Hada, M. Ehara, K. Toyota, R. Fukuda, J. Hasegawa, M. Ishida, T. Nakajima, Y. Honda, O. Kitao, H. Nakai, T. Vreven, K. Throssell, J. A.

Montgomery, Jr., J. E. Peralta, F. Ogliaro, M. Bearpark, J. J. Heyd, E. Brothers, K. N. Kudin, V. N. Staroverov, T. Keith, R. Kobayashi, J. Normand, K. Raghavachari, A. Rendell, J. C. Burant, S. S. Iyengar, J. Tomasi, M. Cossi, J. M. Millam, M. Klene, C. Adamo, R. Cammi, J. W. Ochterski, R. L. Martin, K. Morokuma, O. Farkas, J. B. Foresman, and D. J. Fox, Gaussian, Inc., Wallingford CT, 2016.

(56) Kresse, G.; Furthmüller, J. Efficient Iterative Schemes for Ab Initio Total-Energy Calculations Using a Plane-Wave Basis Set. *Phys. Rev. B.* **54**, 11169–11186 (1996).

(57) Kresse, G.; Furthmüller, J. Efficiency of Ab-Initio Total Energy Calculations for Metals and Semiconductors Using a Plane-Wave Basis Set. *Comput. Mater. Sci.* **6**, 15–50 (1996).

(58) Blöchl, P. E. Projector Augmented-Wave Method. *Phys. Rev. B* **50**, 17953–17979 (1994).

(59) Perdew, J. P.; Burke, K.; Ernzerhof, M. Generalized Gradient Approximation Made Simple. *Phys. Rev. Lett.* **77**, 3865–3868 (1996).

(60) McFarland, E. W.; Metiu, H. Catalysis by Doped Oxides. *Chem. Rev.* **113**, 4391–4427 (2013).

Table

Table 1 is available in the Supplementary Files

Figures

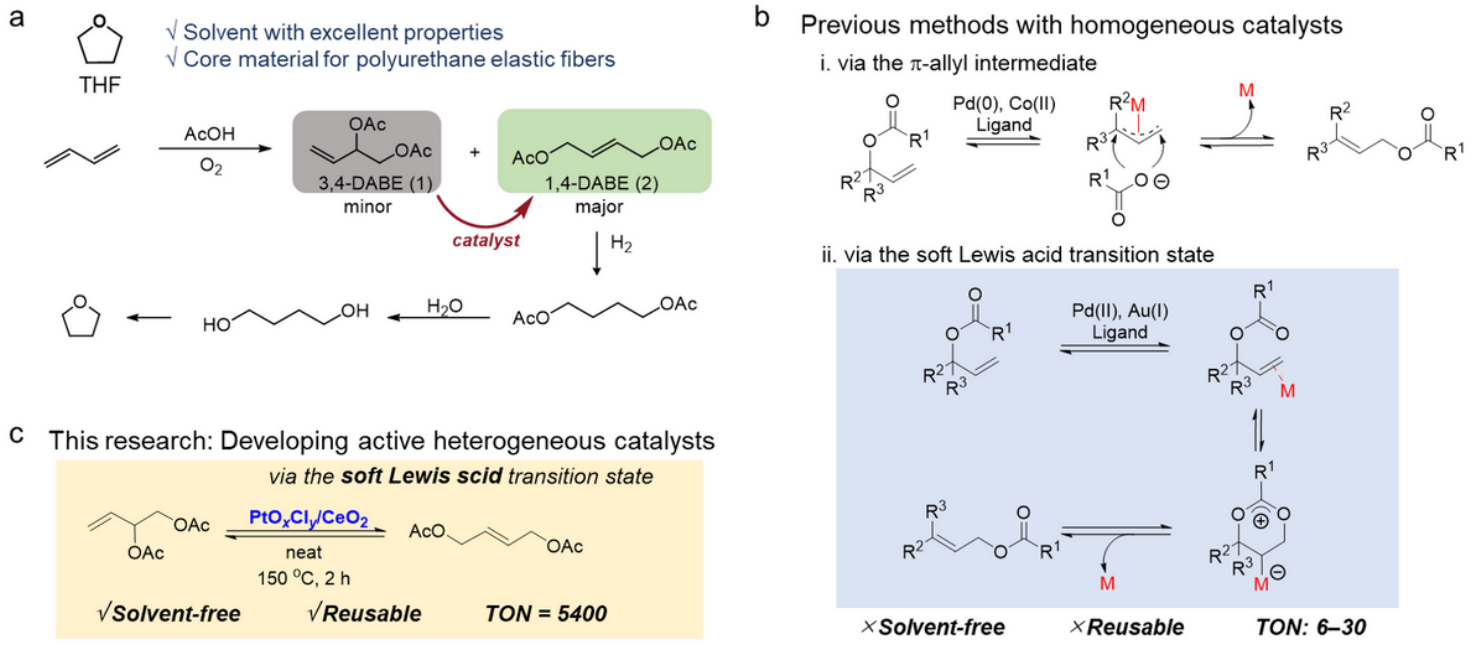

Figure 1

A sustainable transformation: isomerization of allylic esters with efficient soft Lewis acid catalysts. a, A C4 chemical reaction route from buta-1,3-diene. b, Reaction with homogeneous catalysts. c, Research of efficient supported soft Lewis acid catalysts.

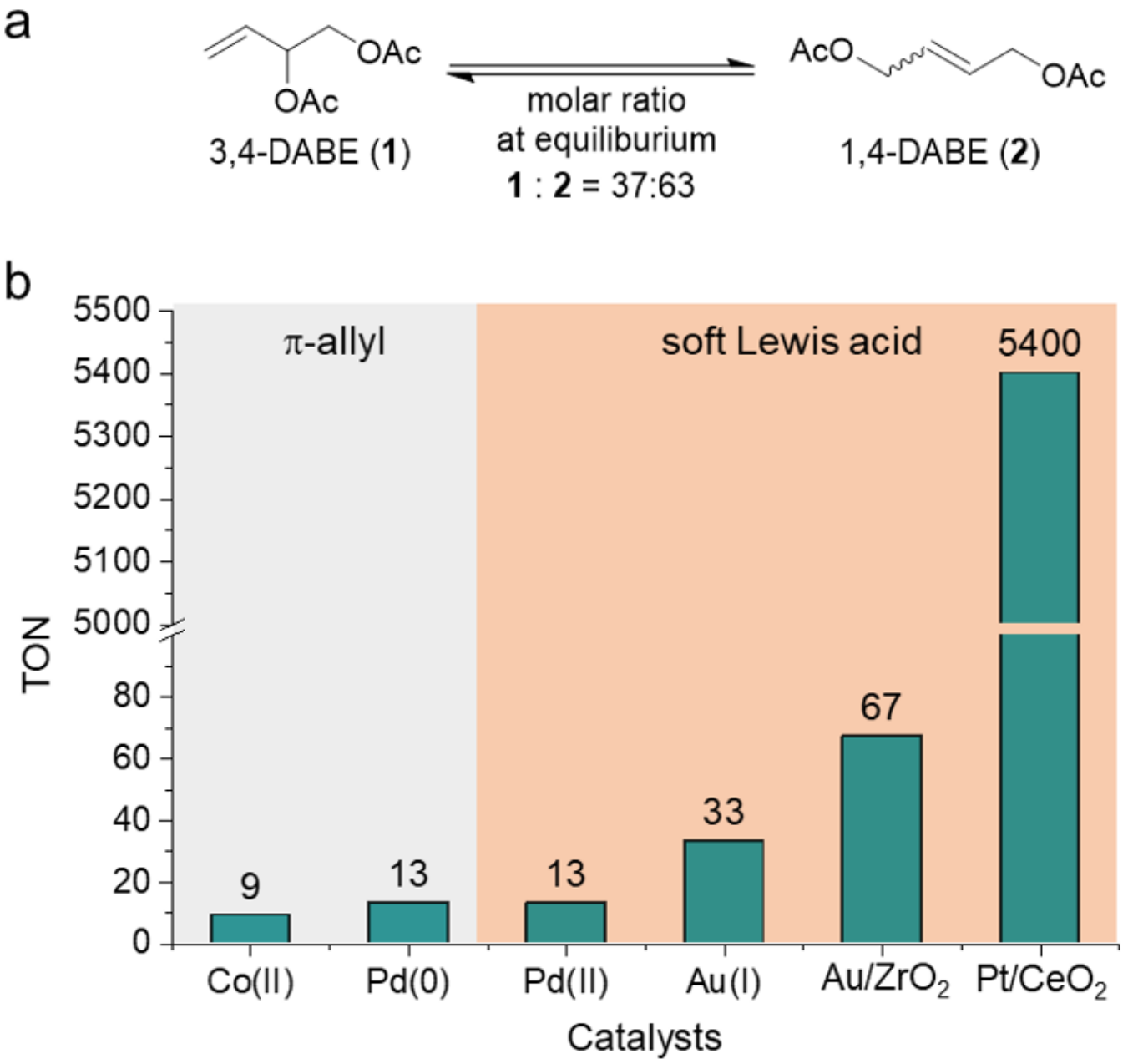

Figure 2

Evaluation of catalytic activity. a, Equilibrium of 3,4-DABE and 1,4-DABE. b, Turnover number (TON) for the catalyst prepared in this study (Au/ZrO2 and Pt/CeO2) and those in previous reports (homogeneous catalysts of Co(II), Pd(0), Pd(II), Au(I))33-36. See Supplementary Table 3 for further details.

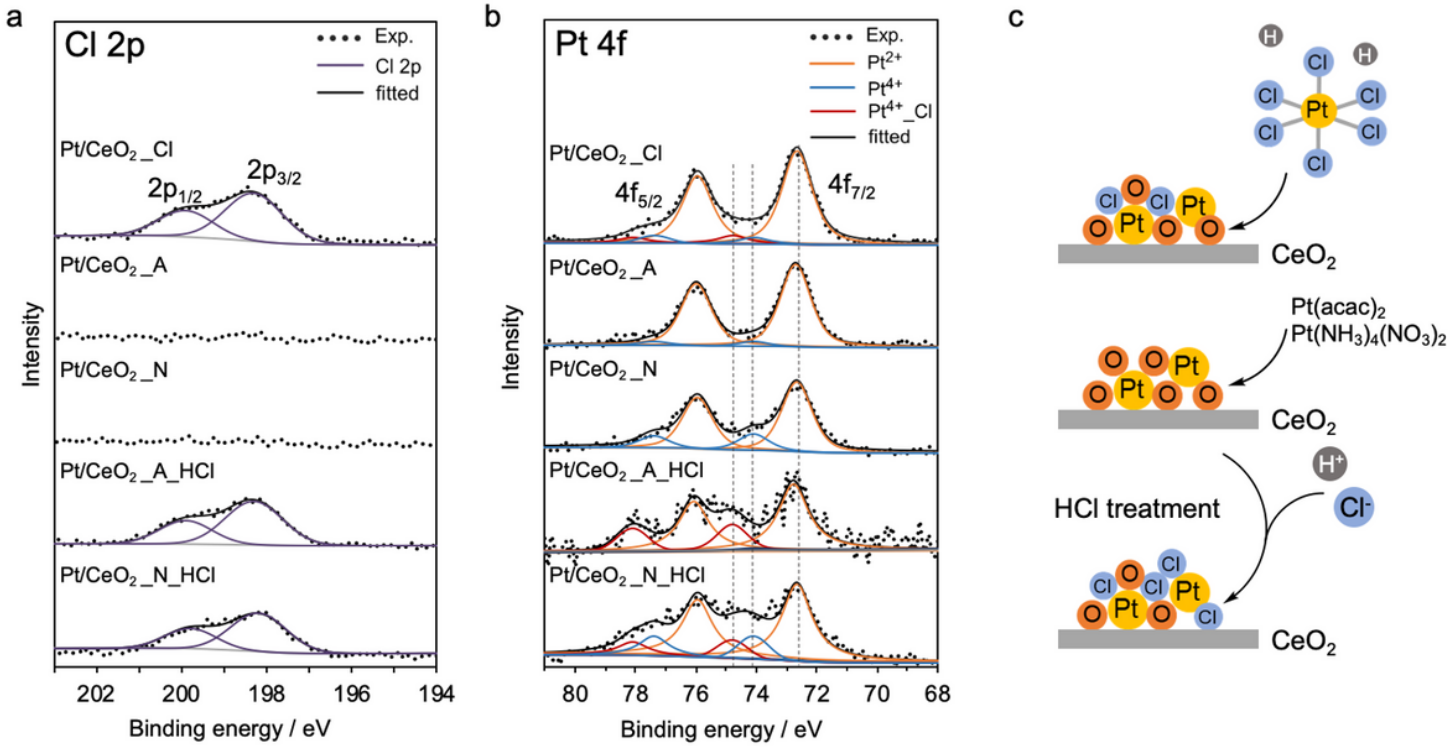

Figure 3

XPS spectra of 1wt% Pt/CeO2 prepared from various precursors or Cl-free catalysts with HCl posttreatment. a, Spectra of Cl 2p. b, Spectra of Pt 4f. c, Simple structural model correlates the XPS spectra of three types of catalysts.

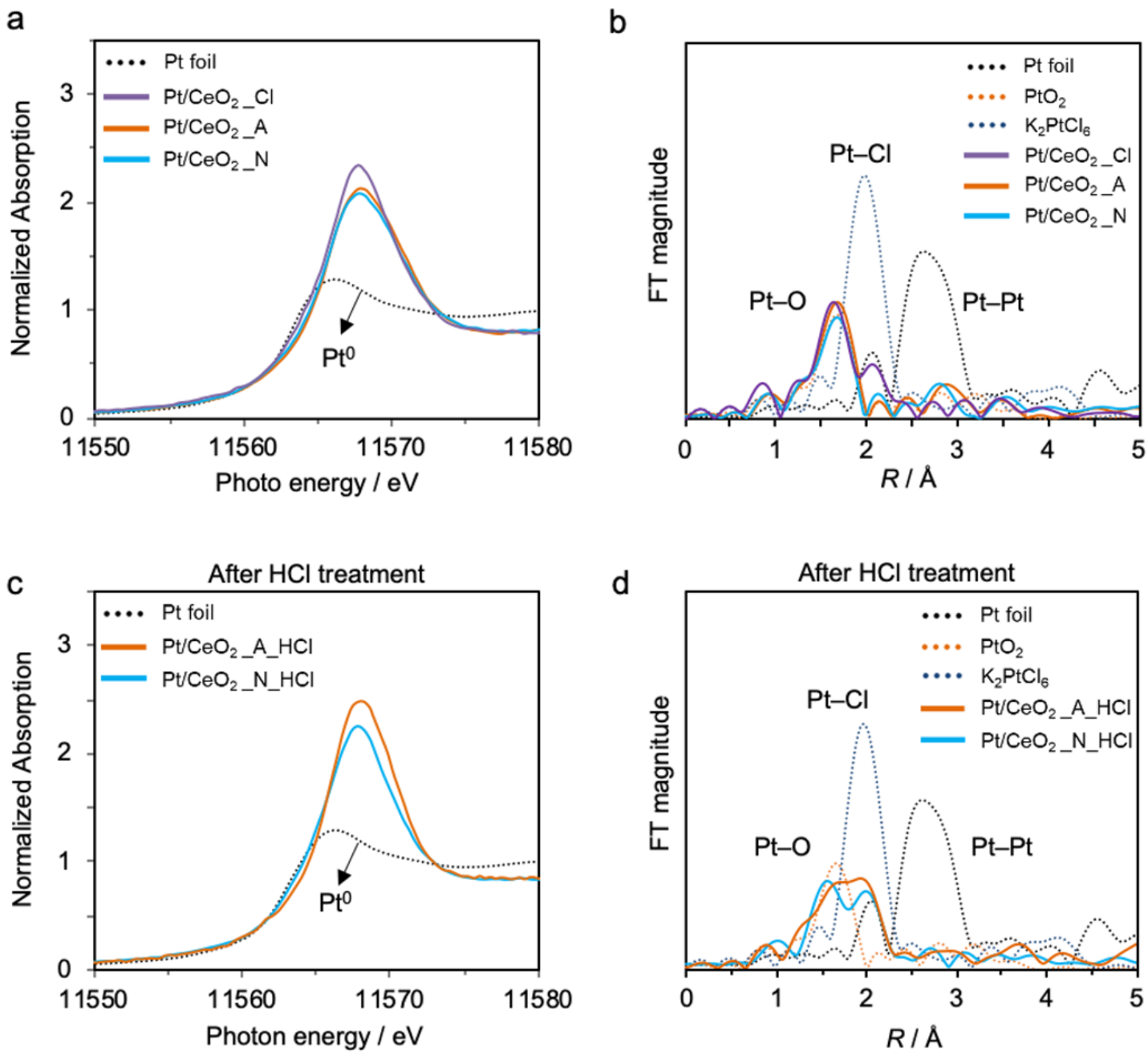

Figure 4

Pt LIII-edge XANES spectra and radial structure functions of Pt/CeO2 (k = 3-13 Å-1). a,b, prepared from different pre-cursors; c,d, HCl-treated Pt/CeO2 prepared from Cl-free precursors.

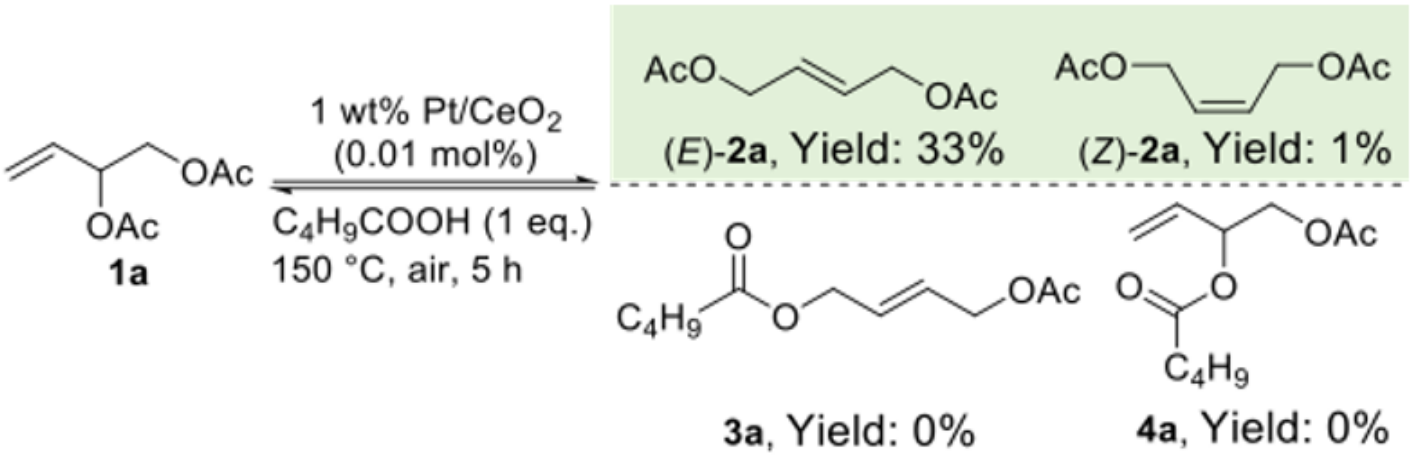

Figure 5

Reaction mechanism investigation by the addition of valeric acid.

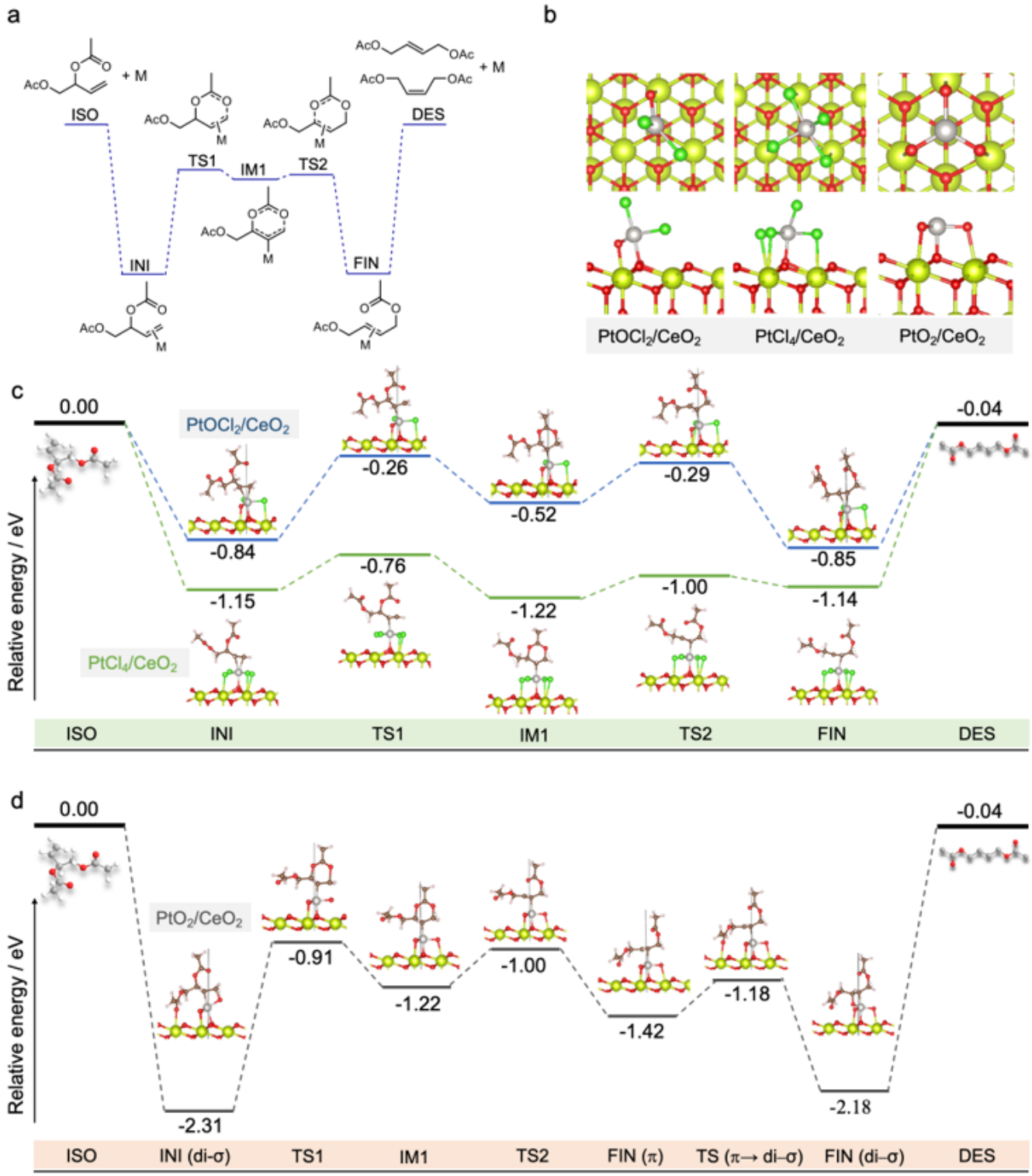

Figure 6

Calculation for isomerization of 3,4-DABE on supported Pt/CeO2 catalysts. a, Basic transition states of the catalytic isomerization of 3,4-DABE on the cluster model. b, Top and side views of atomic Pt-Cl and Pt-O species on CeO2(111). Col-or: Pt, gray; Ce, yellow; oxygen, red; chlorine, green. c, Diagram of the energy calculation of the transition states on the model catalysts PtOCl2/CeO2 and PtCl4/CeO2. d, Diagram of the energy calculation of the transition states on the model cat-alyst PtO2/CeO2.

Supplementary Files

This is a list of supplementary files associated with this preprint. Click to download.

- Table1.png
- PtNCSI0925.docx
- TableofContents.png